A Study of the corona discharge theory for multipoint-plane configurations

by Asep Yoyo Wardaya

Submission date: 03-Feb-2023 05:31PM (UTC+0700)
Submission ID: 2005450054
File name: corona_discharge_theory_for_multipoint-plane_configurations.pdf (508.22K)
Word count: 3917
Character count: 18863

Indian J Phys
https://doi.org/10.1007/s12648-019-01448-0

ORIGINAL PAPER

A study of the corona discharge theory for multipoint–plane configurations

A Y Wardaya[1,2]*, M Nur[1] and J E Suseno[1]

[1]Department of Physics, Faculty of Science and Mathematics, Diponegoro University, Semarang, Indonesia

[2]Master Program of Energy, School of Post Graduate Studies, Diponegoro University, Semarang, Indonesia

Received: 23 November 2017 / Accepted: 31 March 2019

Abstract: This paper presents the numerical calculation of current–voltage (I–V) characteristics that were produced by a corona discharges plasma generator for a multipoint–plane configuration in air and its comparison with the experimental results. The total number of needles in this configuration is $8 \times 4 = 32$ with the distance between the point-to-plane electrodes (denoted as c) as the variable. The I–V characteristic curve of the numerical calculation results matches that of the experimental results for cases with a large distance c (c = 3 and 4 cm), and it shows a large deviation for cases with a small distance c (c = 1 and 2 cm). Differences in the I–V characteristic curve between the experimental and numerical results are due to the symmetrical spread of the ion current from the point-to-plane electrodes, which is more pronounced for larger values of c.

Keywords: Plasma generator; Multipoint–plane configuration; Electric field; Electric current; I–V characteristics

PACS Nos.: 02.30.−f; 02.30.Em; 02.30.Ik; 02.30.Mv; 02.70.−c

1. Introduction

The corona discharge technique has been widely used for various research studies. Some of the papers on various electrode model configurations of corona discharges that try to obtain potential, voltage, or electric current characteristic values include the tip–plane configuration [1], thin bar–needle configuration [2], cylinder–wire–plate configuration [3], sub-millimeter electrode gap configuration [4], point-to-ring configuration [5], and multipoint–plane configuration [6]. However, this paper discusses the current–voltage characteristics from the experimental results. Some other research studies have calculated values related to corona discharges, among which are electrical potential distribution of pin-multi-ring concentric electrodes [7], electrohydrodynamic and wind-ion direction produced by plasma discharge [8], ionic wind generation of needle-to-cylinder electrode model [9], ionic wind generation of multi-electrode model [10], electro hydrodynamic force by a corona discharge [11].

There are also research studies that discuss the direct application of the corona discharge electrode configuration; cold large-diameter plasma jet of a triple electrode model [12], electric potential distribution of various electrode models [13], and laser-induced streamer corona discharge of a needle-to-plate electrode model [14].

This research is considered an extension of the work reported by Jaworek and Krupa [6] for the case of comparing the numerical calculation and experimental results of voltage and electric current characteristics generated by a corona discharge from plasma electrodes using a multipoint configuration. According to Sigmond [15], a large electric field generation along with a saturated current in the form of a corona discharge that in turn produces corona plasma which is due to the sharp end of one of the electrodes and the asymmetrical shape of both electrodes.

In this study, we use a model of a multipoint–plane configuration that consists of two perpendicular plates on one of which $m \times n$ number of needles is attached, as shown in Fig. 1.

As seen in Fig. 1, the needle length is b, inter-needle space is a, and distance between the point-to-plane electrodes is c. Hence, the distance between the two thin plates

*Corresponding author, E-mail: asepyoyowardayafisika@gmail.com

Published online: 20 April 2019

© 2019 IACS

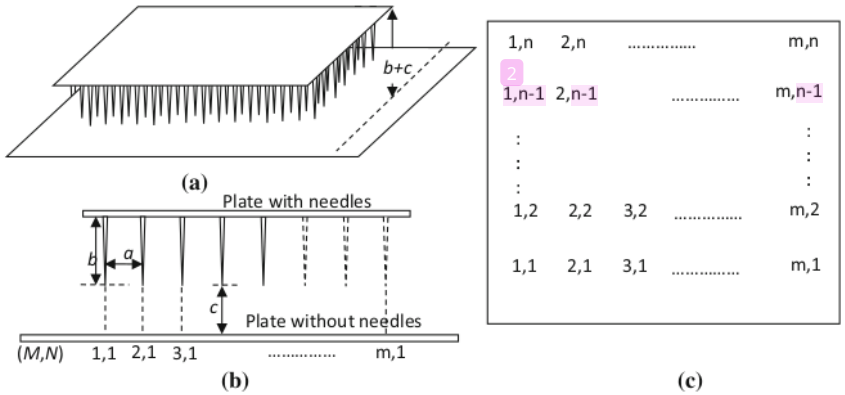

Fig. 1 Model of the multipoint–plane configuration consisting of two parallel plates on one of which $m \times n$ needles are attached. The inter-needle distance is a, needle length is b, and distance between the point-to-plane electrodes is c. (**a**). 3D representation of the electrode model. (**b**). Side view of the electrode model. (**c**). Top view of the location of $m \times n$ needles (marked $\times$)

is $b + c$. The experiment of the corona discharge for the multipoint–plane configuration uses DC voltage; with a positive polarity position at the point position and negative polarity at the plane position.

2. Electric field intensity

The electric field generated by the corona discharge from the point–plane configuration can be calculated using a formula [1] that transforms hyperbolic coordinates into Cartesian coordinates as follows:

$$E(x,y,z) = \frac{[V/\ln(\frac{2}{\varepsilon})]}{\sqrt{c^2\cos^4\xi + x^2 + y^2}}, \tag{1}$$

where the hyperbolic coordinates (η, ξ, ψ) relate to the 3D Cartesian coordinates as follows [1]:

$$x = -c\cos\xi\sinh\eta\sin\psi; \quad y = -c\cos\xi\sinh\eta\cos\psi; \quad z = c\sin\xi\cosh\eta, \tag{2}$$

where [1]

$$\cos^2\xi = \frac{u + \sqrt{u^2 + 4c^2(x^2+y^2)}}{2c^2}, \tag{3}$$

and [1]

$$u = c^2 - (x^2 + y^2 + z^2) = c^2\cos^2\xi - \frac{(x^2+y^2)}{\cos^2\xi}, \tag{4}$$

and V is the input voltage.

To calculate certain positions on the plate without the needle against the needle tip position, we perform the calculation as if the upper part of Fig. 1.a only has one needle at position (2, 2) in Fig. 1.c. The position without a needle is designated as "filled circle," whereas the position with a needle is assigned as $\times$, as shown in Fig. 2.a, for a 2D representation in the xz coordinates. However, seen from the z-axis, both position marks "filled circle" and $\times$ for coordinate (2, 2) will coalesce as A_{00}. Therefore, a combination of those two marks in Fig. 2.b can simply be assigned as ($\times$).

In Fig. 2.a, a needle of length b (ending at point P) is attached on the plate (marked $\times$). The other points (A_{00}, A_{10}, A_{20}, ...) are at a distance of $b + c$ from the plate with the needle, or points A_{00}, A_{10}, A_{20}, ... have a distance of $z = \varsigma; \varsigma \ll 1$ from the x-axis, where c is the distance from the needle tip to the plate without the needle.

The electric field generated by a needle electrode voltage source at point P with the coordinate $\xi = \frac{1}{2}\pi - \varepsilon$, where $\varepsilon \ll 1$, and $\eta = 0$ (as $x = y = 0$, $z \sim c$, $u \sim 0$), can be expressed similarly to equation [1]:

$$E_P = E\left(\xi = \frac{1}{2}\pi - \varepsilon, \eta = 0\right) = \frac{[V/\ln(\frac{2}{\varepsilon})]}{c\cos^2(\frac{1}{2}\pi - \varepsilon)}, \tag{5}$$

where the relationship of the coordinate η and variables x and y is defined as follows [1]:

$$\eta = \tanh^{-1}\left\{\frac{\sqrt{x^2+y^2}}{z}\tan\left(\frac{1}{2}\pi - \varepsilon\right)\right\}. \tag{6}$$

Equation (6) indicates a high electric field at the needle tip (point P) due to the value of $\cos^2(\frac{1}{2}\pi - \varepsilon) \ll 1$.

For the case at point A_{00} on the z-axis, with the distance c at the needle tip and its position at $z = \varsigma; \varsigma \ll 1; z \to 0$, the resulting electric field at point A_{00} at position $x = y = 0$ or $\eta = 0$ is [1] as follows:

$$E_{00}(x = y = 0, z) = \lim_{z\to 0}\frac{[cV/\ln(\frac{2}{\varepsilon})]}{(c^2 - z^2)}. \tag{7}$$

At another point $A_{\mu\nu}$ with $x = \mu a$ and $y = \nu a$, $\mu,\nu = 0, \pm 1, \pm 2,\ldots$, the electric field induced by a point–plane electrode voltage source with the needle coalescing with the z-axis and its point at point P is as follows:

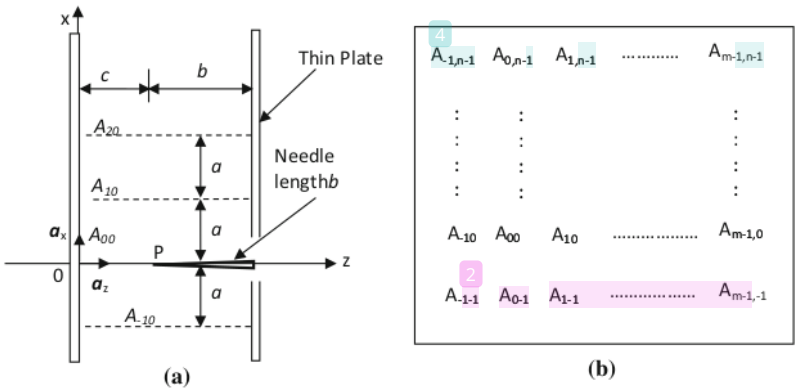

Fig. 2 (**a**) Description of P points, A_{00}, A_{10}, A_{20} (marked "filled circle") on the 2D xz-plane ($y = 0$ and $z = \varsigma$, $\varsigma \ll 1$) that is induced by the electric current from the point–plane electrodes located in the positions marked (×). (**b**) Full description of the points on the xy-plane from the z point of view without taking P into account, A_{-10}, A_{00}, A_{10}, etc. Observed from z, the position of A_{00} ("filled circle") coalesces with needle position (×), so that mark × is sufficient

$$E_{\mu\nu}(x=\mu a, y=\nu a, z=\varsigma)=\frac{[2cV/\ln(\frac{z}{\varsigma})]}{\sqrt{U_{\mu\nu}^2+4(\mu^2+\nu^2)c^2a^2}}, \tag{8}$$

where

$$U_{\mu\nu}=2c^2\cos^2\xi=u_{\mu\nu}+\sqrt{u_{\mu\nu}^2+4c^2a^2(\mu^2+\nu^2)}, \tag{9}$$

and

$$\begin{aligned} u_{\mu\nu}&=\lim_{z\to 0}\left[c^2-\left(x^2+y^2+z^2\right)\right]\\ &=\lim_{z\to 0}\left[c^2-\left(\mu^2+\nu^2\right)a^2-z^2\right]. \end{aligned} \tag{10}$$

The following commutative relationship with absolute value applies

$$\begin{aligned} &E_{\mu\nu}=E_{\nu\mu}=E_{|\mu||\nu|};\quad U_{\mu\nu}=U_{\nu\mu}=U_{|\mu||\nu|};\\ &u_{\mu\nu}=u_{\nu\mu}=u_{|\mu||\nu|}. \end{aligned} \tag{11}$$

3. Electric field superposition

When there are $m \times n$ needle electrodes inducing a homogeneous electric field at certain points (Fig. 1c), the electric field inducing those points can be calculated using the concept of the electric field vector superposition that stems from those needles. In general, the magnitude of the electric field can be used for all points at $z = \zeta$, therefore the calculation for the individual vector electric field where $x = \mu a$, $y = \nu a$ and $z = \zeta << 1$, is as follows:

$$\mathbf{E}_{\mu\nu}(x,y,z)=E_{\mu\nu}(\mu a,\nu a,\varsigma)\frac{\left\{x_N\mathbf{a}_x+y_N\mathbf{a}_y-c\mathbf{a}_z\right\}}{\sqrt{x_N^2+y_N^2+c^2}}, \tag{12}$$

where x_N, y_N, and $z_N = -c$, which is the length of a 3D vector from the needle tip to certain positions (M, N) (Fig. 1.b). The electric field on the plate without a needle (plane xy) will be calculated. (Point A_{00} is always at distance c from the needle tip.) The total electric field at point (M, N) is a superposition of the individual electric fields that consist of $A \times B$ needle electrodes that induce the point (M, N), with $m \times n$ being the total number of needles; hence, $A \times B \le m \times n$ can be written as follows:

$$\begin{aligned} (\mathbf{E}_T)_{\mathbf{MN}}=&\sum_{\mu=0}^{A-1}\sum_{\nu=0}^{B-1}\mathbf{E}_{\mu\nu}(x,y,z),\quad M=1,2,\ldots,m.\quad \text{and}\\ &N=1,2,\ldots,n. \end{aligned} \tag{13}$$

Some indexing rules apply:

1. The index (M, N) is a fixed position index on the xy-plane that relates to the number of needles ($m \times n$).
2. The index μ,ν is the variable position index from point coordinate A_{ij} at position ($x = \mu a$, $y = \nu a$, $z = \zeta$) from the central coordinate (0, 0, 0) point of view, in which the reference point A_{00} is a position at distance c from the needle tip at the fixed index needle position (M, N).
3. The notations x_N, y_N, and $z_N = -c$ are vector coordinates of the needle positions that stem from the needle tips and end at the points where the electric field is calculated on the plate without a needle (xy-plane).

The total electric field at certain positions (M, N) at distance c from the tip of the needles induced by the electric field generated by $A \times B$ needle electrodes (the total number of which is $m \times n$) based on Eq. (13) is as follows:

$$\begin{aligned} (\mathbf{E}_T)_{\mathbf{MN}}=&\sum_{\mu=0}^{A-1}\sum_{\nu=0}^{B-1}\left[E_{|M-1-\mu|,|N-1-\nu|}\right]_{\mu+1,\nu+1}\\ &\frac{\left\{(M-1-\mu)a\mathbf{a}_x+(N-1-\nu)a\mathbf{a}_y-c\mathbf{a}_z\right\}}{\sqrt{((M-1-\mu)a)^2+((N-1-\nu)a)^2+c^2}}, \end{aligned} \tag{14}$$

where $M = 1, 2, 3,\ldots, m$ and $N = 1, 2, 3,\ldots, n$. This equation has electric field notation $E_{|M-1-\mu|,|N-1-\nu|}$ which relates to Eq. (11).

We can consider that there is an arrangement of $m \times n$ needle electrodes as shown in Fig. 1.c. To calculate the electric field produced by each needle, at distance c from the needle tip, Eq. (14) is used. On the other hand, to calculate the total electric current produced by all needles, vector addition from each electric field unit in Eq. (14) must be performed. The total electric field resulting from all needles on the x- and y-axes will cancel each other out due to the symmetrical property, and what is left is the electric field components on the z-axis that will later be calculated.

Equation (14) describes the electric field resulting from the ions that flow to the points at distances $x_\alpha = \alpha a$ and $y_\beta = \beta a$, with $\alpha = 0, 1, 2, \ldots, A-1$ and $\beta = 0, 1,2, \ldots, B-1$, where A and B are the maximum points on the plate surface that exposed by the ion current at the x and y coordinates, respectively, in discrete numbers. These ion currents will flow from the needle tip to the plate surface with the maximum plate area of $xy = (A-1)(B-1)a^2$. Because the ion current flux has symmetrical, homogeneous, and continuous properties in the plane configuration, the discrete characteristics (summation form) in Eq. (14) become the continuous characteristics (integration form) of the electric field quantity that can be solved using Eq. (15);

$$(E_z)_{m\times n} = \frac{c}{a^2}\sum_{\alpha=0}^{A-1}\sum_{\beta=0}^{B-1}\int_{x=0}^{a\alpha} \mathrm{d}x_\alpha \int_{y=0}^{a\beta} \mathrm{d}y_\beta \frac{\left[VK_{|\alpha||\beta|}/\ln\left(\frac{2}{\varepsilon}\right)\right]}{\left(x_\alpha^2 + y_\beta^2 + c^2\right)} \tag{15}$$

Substitution from 2D Cartesian coordinates to the polar coordinates results in the following:

$$(E_z)_{m\times n} = \frac{c}{a^2}\left[\frac{VK_{|\alpha||\beta|}}{\ln\left(\frac{2}{\varepsilon}\right)}\right]\sum_{\alpha=0}^{A-1}\sum_{\beta=0}^{B-1}\int_{\rho=0}^{a\sqrt{\alpha^2+\beta^2}} \frac{\rho_{\alpha\beta}}{\left(\rho_{\alpha\beta}^2 + c^2\right)}\mathrm{d}\rho_{\alpha\beta}\int_{\phi=0}^{2\pi}\mathrm{d}\phi, \quad \rho_{\alpha\beta}^2 = x_\alpha^2 + y_\beta^2, \tag{16}$$

and this generates the electric field given by the following:

$$(E_z)_{m\times n} = \frac{\pi c}{a^2}\left[\frac{V}{\ln\left(\frac{2}{\varepsilon}\right)}\right]\sum_{\alpha=0}^{A-1}\sum_{\beta=0}^{B-1} K_{|\alpha||\beta|}\ln\left|\frac{a^2\left(\alpha^2+\beta^2\right)+c^2}{c^2}\right|. \tag{17}$$

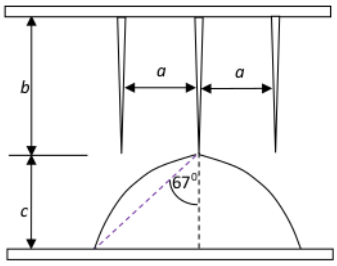

Fig. 3 Maximum angular deviation of the electric field from the induced point location to the perpendicular direction of the needle is around 67°

4. Angle of plasma ion flow

We note that not all points at positions $A_{\mu\nu}$, $\mu,\nu = 0, \pm 1, \pm 2,\ldots$ can be induced by the electric field. According to Nur et al. [8], the angular deviation of the plasma ion flow from the point location induced by the electric field to the perpendicular direction of the needle is around 60°, up to a maximum of 67°, as shown in Fig. 3.

The relationship of θ and the position $A_{|\alpha||\beta|}$ can be calculated with the following equation:

$$\theta = \tan^{-1}\left\{\frac{a}{c}\sqrt{\alpha^2+\beta^2}\right\} \le 67^\circ, \quad \text{at position } A_{|a||b|}. \tag{18}$$

To verify the numerical simulations, we conducted an experiment to determine the relationship between the electric current I and voltage source V using a plasma discharge with multipoint–plane configuration, which has been performed at the Radiation Physics Laboratory at Diponegoro University. The needles were arranged in an $8 \times 4 = 32$ needle formation with $a = 0.8068$ cm, $b = 0.018$ cm, and c was varied at 1 cm; 2 cm; 3 cm; and 4 cm. The overall value of $K_{\alpha\beta}$ for the 8×4 needle configuration is as follows:

$$K_{00} = 32; K_{|0||\beta|} = K_{|\alpha||0|} = 64 \text{ and } K_{|\alpha||\beta|} = 128 \text{ for } \alpha, \beta = 1, 2, \ldots, 7. \tag{19}$$

The values of $A_{|\alpha||\beta|}$ index couple (α, β) and position number $K_{|\alpha||\beta|}$ for each variation of c, [taking Eq. (18) into account] are given in Table 1.

5. Induced current

In the case of the point–plane configuration, the charge Q induced on the plane electrode becomes [1] the following:

Table 1 Values of position $A_{|\alpha||\beta|}$, index couple (α, β), and position number $K_{|\alpha||\beta|}$ for varied c

No.	C	Position	(α, β)	$K_{\|\alpha\|\|\beta\|}$
1.	1 cm	$A_{00}, A_{|0||1|}, A_{|1||0|}, A_{|1||1|}, A_{|1||2|}, A_{|2||1|}, A_{|2||2|}$	(0,0); (0, 1); (1,0); (1, 1); (1, 2); (2, 1); (2, 2)	$K_{|0||0|}, K_{|0||1|}, K_{|1||0|}, K_{|1||1|}, K_{|1||2|}, K_{|2||1|}, K_{|2||2|}$
2.	2 cm	$A_{|0||0|}, \ldots, A_{|3||3|}, A_{|3||4|}, A_{|3||5|}, A_{|4||3|}, A_{|5||3|}$	(0,0); (0, 1); (1,0); …; (3, 3); (3, 4); (3, 5); (4, 3); (5, 3)	$K_{|0||0|}, \ldots, K_{|3||3|}, K_{|3||4|}, K_{|3||5|}, K_{|4||3|}, K_{|5||3|}$
3.	3 cm	$A_{00}, A_{|0||1|}, A_{|1||0|}, A_{|1||1|}, \ldots, A_{|6||6|}, A_{|7||6|}, A_{|6||7|}$	(0,0); (0, 1); (1,0); …; (6, 6); (7, 6); (6, 7)	$K_{|0||0|}, K_{|0||1|}, K_{|1||0|}, \ldots, K_{|6||6|}, K_{|7|6|}, K_{|6||7|}$
4.	4 cm	$A_{00}, A_{|0||1|}, A_{|1||0|}, A_{|1||1|}, \ldots, A_{|7||6|}, A_{|6||7|}, A_{|7||7|}$	(0,0); (0, 1); (1,0); …; (6, 6); (7, 6); (6, 7); (7, 7)	$K_{|0||0|}, K_{|0||1|}, K_{|1||0|}, \ldots, K_{|6||6|}, K_{|7|6|}, K_{|6||7|}, K_{|7||7|}$

$$Q = \frac{V(\xi) - V}{V} q, \tag{20}$$

where V is the potential of the point electrode and q is the charge of the electric flux lines coming from the multipoint to the plane configuration as defined in Eq. (20), and the induced current yields the following (Fig. 4):

$$i = -\frac{dQ}{dt} = -\frac{q}{V}\frac{dV(\xi)}{ds}\frac{ds}{dt} = \mu_0 \frac{q}{V} E^2. \tag{21}$$

According to Halliday et al. [16], the electric field strength at point B can be written as follows:

$$E_Q = \frac{q}{4\pi\varepsilon_0 c}\frac{1}{(b+c)}. \tag{22}$$

When the results from the work by Coelho and Debeau [1] are used as a comparison, the electric field strength at B located at distance c from the point electrode can be written as follows:

$$E_Q \cong \frac{V}{c \ln\left(\frac{2}{\in}\right)}. \tag{23}$$

Using Eqs. (22) and (23), charge q is yielded as follows:

$$q = \frac{4\pi\varepsilon_0 (b+c) V}{\ln\left(\frac{2}{\in}\right)}. \tag{24}$$

The electric current from the multipoint–plane configuration with 32 needles ($N = 32$) can be calculated using Eqs. (17), (21), and (24) as follows:

$$\begin{aligned} i &= -N\frac{\mathrm{d}Q}{\mathrm{d}t} \\ &= \mu_0 N \frac{4\pi^3 \varepsilon_0 (b+c) c^2 V^2}{a^4 \ln^3\left(\frac{2}{\in}\right)} \\ &\quad \left\{ \sum_{\alpha=0}^{A-1} \sum_{\beta=0}^{B-1} K_{|\alpha||\beta|} \ln \left| \frac{a^2(\alpha^2+\beta^2)+c^2}{c^2} \right| \right\}^2 \\ &\quad \text{with} \quad \in << < 1, \end{aligned} \tag{25}$$

where μ_0 and ε_0 are the mobility ($4\pi \times 10^{-7}$ Wb/A.m) and permittivity (8.85×10^{-12} F/m) at the vacuum space, respectively.

6. Results and discussion

In the simulation graphs for the electric current I and voltage V, we use Table 1 and Eq. (25) for different values of c (1, 2, 3, and 4 cm) (Fig. 5). These simulation graphs are compared with experiment graphs of the same variations of electric current I and voltage V;

A theory of corona discharge with multipoint–plane configuration has been discussed. The calculations of the

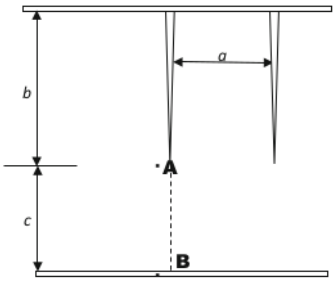

Fig. 4 Electric field calculation on the plane electrode (B) positioned at distance c from the point electrode (A)

electric field and saturated current generated from this configuration when input voltage V is applied have also been elaborated. The calculation of the total electric field resulting from $m \times n$ needle electrodes must be done using the concept of the electric field vector superposition. This research employs an arrangement of 8×4 needle electrodes with varied distances between the point-to-plane electrodes (c) at 1, 2, 3, and 4 cm.

The resulting graphs show that the simulation results are closer to the experiment results when the distance c is larger, especially for c at 3 cm and 4 cm. A narrower c causes an asymmetrical and inhomogeneous ion flow in which some areas are flooded with more ions than predicted. For a higher c, the symmetrical and homogeneous ion flow is closer to the experimental results. This causes an electric current reading that is closer to the expected value. Moreover, a narrower c does not allow the maximum electric field deviation angle from the induced point location to the perpendicular needle position, which may reach 67°, while greater c allows this to take place, hence, almost all ion flow that stems from the needle electrodes reaches all the designated points on the plane without the needles, and in turn, yields a greater electric field. Another influencing factor for the electric current reading is the shape of the needle with a sharpness no closer than 0°, which is the ideal condition for electric field calculation.

These statements can be explained as follows: Equation (14) shows the 3D vector of the ion current flow model that flows from the needle tip to the bottom plate with a parabolic shape as shown in Fig. 3. To simplify Eq. (14), we assume that the ion current flows symmetrically so that the flowing 3D vector will be changed to one direction in the upright axis (z-axis) because the ion current direction at the xy-plane will be a symmetrical circle; therefore, it will eliminate the others. Another assumption is that the ion current in the direction of the z-axis will be homogenously distributed and close to continuously flowing, so that the vector and discrete (summation) characteristics in Eq. (14) are changed to continuous (integration) and scalar characteristics (only in the direction of the z-axis) in Eq. (15), where Eq. (15) is part of Eq. (25). Therefore, the

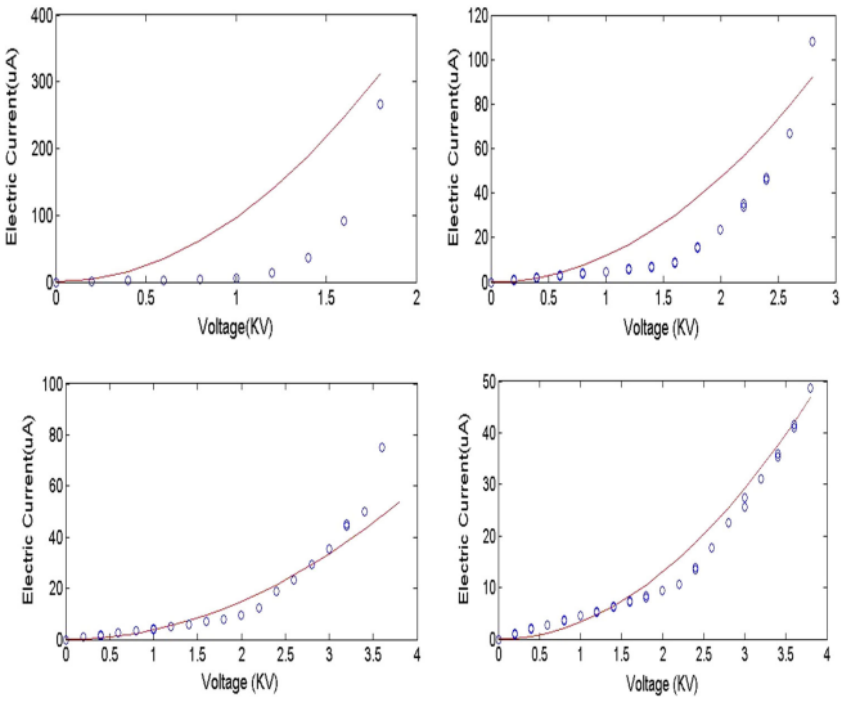

Fig. 5 Graphs of the relationship between the electric current I and voltage source V obtained from the $8 \times 4 = 32$ needle electrode configuration, limited to 67° for the maximum deviation angle for $a = 0.8068$ cm, $b = 0.018$ cm, and varied c at 1, 2, 3, and 4 cm. Blue circles indicate the experiment results. Red lines show simulation results from Eq. (25)

conditions of homogenous continuity and symmetry will be better for an increased distance from the multipoint–plane to the bottom plate surface, so that the mathematical simulation will match the results of the experiment at a greater value of c.

7. Conclusion

The current–voltage (I–V) characteristics that were produced by the corona discharge plasma generator for the multipoint–plane configuration in the air could demonstrate the performance of a device. The total electric field inducing these points could be calculated using the concept of the electric field vector superposition that stems from these needles. The total number of needles in this configuration is $8 \times 4 = 32$, and there is a variation of distance c, which is the distance between the point-to-plane electrodes. The comparison between the numerical simulation and experimental results indicated that the I–V characteristic curve is simulated better for longer distances between the point-to-plane electrodes, which is roughly longer than 3 cm; due to better symmetry and homogeneity of the ion current flows from the multipoint-plane to the plane configuration.

References

[1] R Coelho and J Debeau *J. Phys. D: Appl. Phys.* **4** 1266 (1971)
[2] A Y Wardaya and M Nur *Berkala Fisika UNDIP* **18** 67 (2015)
[3] L M Dumitran, L Dascalescu, P V Notinger and P Atten *J. Electrost.* **65** 758 (2007)
[4] R Tirumala, Y Li, D A Pohlman and D B Go *J. Electrost.* **69** 36 (2011)
[5] V T Daua,T X Dinhb, TTerebessyc and T T Bui *Sens. Actuators A Phys.* **244** 146 (2016)
[6] A Jaworek and A Krupa *J. Electrost.* **38** 187 (1996)
[7] Sumariyah, Kusminarto, A Hermanto, P Nuswantoro, Z Muhlisinand E Setiawati *Proced Environ Sci* **23** 260 (2015), Int. Conf. on Tropical and Coastal Region Eco-Development (2014).
[8] M Nur, A H Azzulkha, M Restiwijaya, Z Muchlisin and Sumariyah *Adv. Phys. Theories Appl.* **30** 55 (2014)
[9] [9] L Li, S J Lee, W Kimand D Kim *J. Electrost.* **73** 125 (2015)
[10] M J Johnson, R Tirumala and D B Go *J. Electrost.* **74** 8 (2015)
[11] E Moreau, N Benard, F Alicalapa and A Douyere *J. Electrost.* **76** 194 (2015)
[12] S Wang, J Zhang, G Li, and D Wang *Vacuum* **101** 317 (2014)
[13] A Reguig, A Bendaoud, B Neagoe, Y Prawatyaand and L Dascalescu *J. Electrost.* **82** 55 (2016)
[14] S Kanazawa, TIto, YShuto, T Ohkubo, Y Nomotoand and J Mizeraczyk *J. Electrost.* **55** 343 (2002)
[15] R S Sigmond *J Appl Phys* **53** 891 (1982)
[16] D Halliday, R Resnick and J Walker *Fundamentals of Physics* (New York: John Wiley & Sons 7th. Edition) (2005)

Publisher's Note Springer Nature remains neutral with regard to jurisdictional claims in published maps and institutional affiliations.

A Study of the corona discharge theory for multipoint-plane configurations

ORIGINALITY REPORT

6%	3%	4%	0%
SIMILARITY INDEX	INTERNET SOURCES	PUBLICATIONS	STUDENT PAPERS

PRIMARY SOURCES

1	Tae-Hee Lee, Jun-Hee Park, Dal-Hun Yang, Jang-Ho Jay Kim, Norhazilan Bin Md. Noor. "Material enhancements of newly developed stiff type polyurea for retrofitting of concrete structures", Case Studies in Construction Materials, 2022 Publication	1%
2	pt.scribd.com Internet Source	<1%
3	Edoardo Fusella, Alessandro Cilardo. "Lattice-Based Turn Model for Adaptive Routing", IEEE Transactions on Parallel and Distributed Systems, 2018 Publication	<1%
4	idoc.pub Internet Source	<1%
5	Clemens Fuchs, Volker Ziegler. "On a Family of Thue Equations Over Function Fields", Monatshefte für Mathematik, 2005 Publication	<1%

6	ronl.org Internet Source	<1 %
7	prints.iiap.res.in Internet Source	<1 %
8	Peter Ballett, Stephen F. King, Christoph Luhn, Silvia Pascoli, Michael A. Schmidt. "Testing atmospheric mixing sum rules at precision neutrino facilities", Physical Review D, 2014 Publication	<1 %
9	cardinalscholar.bsu.edu Internet Source	<1 %
10	doi.org Internet Source	<1 %
11	research.thea.ie Internet Source	<1 %
12	Edmund Chadwick. "A slender-body theory in Oseen flow", Proceedings of The Royal Society A Mathematical Physical and Engineering Sciences, 08/08/2002 Publication	<1 %
13	Yifei Guan, Ravi Sankar Vaddi, Alberto Aliseda, Igor Novosselov. "Analytical model of electro-hydrodynamic flow in corona discharge", Physics of Plasmas, 2018 Publication	<1 %
	www.science.gov	

14	Internet Source	<1%
15	dokumen.pub Internet Source	<1%
16	epdf.pub Internet Source	<1%
17	slideheaven.com Internet Source	<1%
18	text.xemtailieu.net Internet Source	<1%
19	Jean François Walhin. "Bivariate ZIP Models", Biometrical Journal, 05/2001 Publication	<1%
20	Jingguo Qu, Minjun Zeng, Dewei Zhang, Dakai Yang, Xiongwei Wu, Qinlong Ren, Jian-Fei Zhang. "A review on recent advances and challenges of ionic wind produced by corona discharges with practical applications", Journal of Physics D: Applied Physics, 2021 Publication	<1%

Exclude quotes	On	Exclude matches	Off
Exclude bibliography	On		

A Study of the corona discharge theory for multipoint-plane configurations

GRADEMARK REPORT

FINAL GRADE

/0

GENERAL COMMENTS

Instructor

PAGE 1

PAGE 2

PAGE 3

PAGE 4

PAGE 5

PAGE 6

PAGE 7